Electronic Supplementary Material (ESI) for RSC Advances.

Supplementary Information for

Several orders of magnitude increase in hydraulic permeability of flow-through capacitive deionization electrodes via laser perforations

Eric N. Guyes[a], Anastasia Simanovski[a], Matthew E. Suss[a,*]

[a]*Faculty of Mechanical Engineering, Technion – Israel Institute of Technology, Haifa 32000, Israel*

**Email: mesuss@tx.technion.ac.il*

SI1: SEM images of the laser perforations

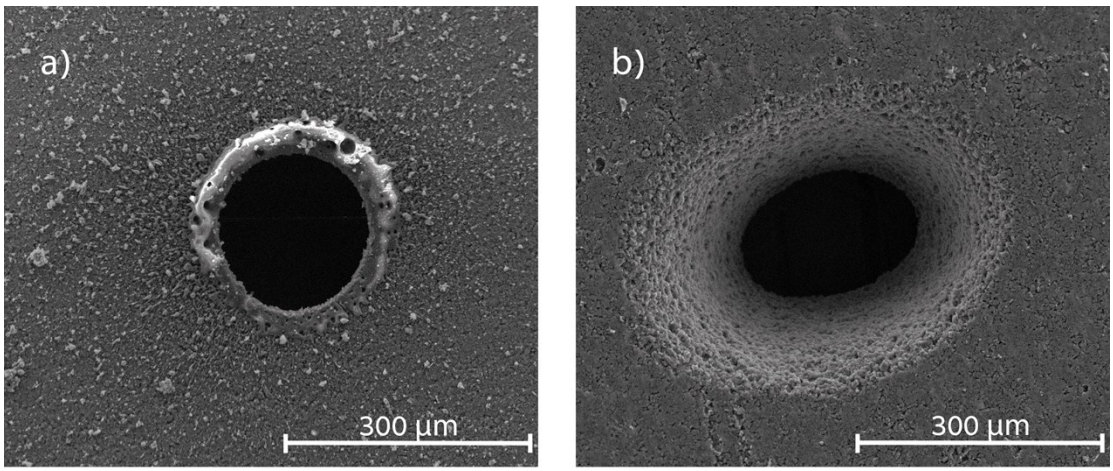

Figure S1 – a) SEM image of a representative laser perforation, showing the aperture along the surface furthest from the laser head during the cutting operation. The aperture is circular with a roughly 200-µm diameter, and the white-tinged substance surrounding the perforation is assumed to be the PTFE binder, which was melted during laser cutting. b) A representative aperture along the surface closest to the laser head during the cutting operation. The aperture is elliptical and greater than 200 µm in characteristic size.

SI2: CDI cell schematic and pressure modeling

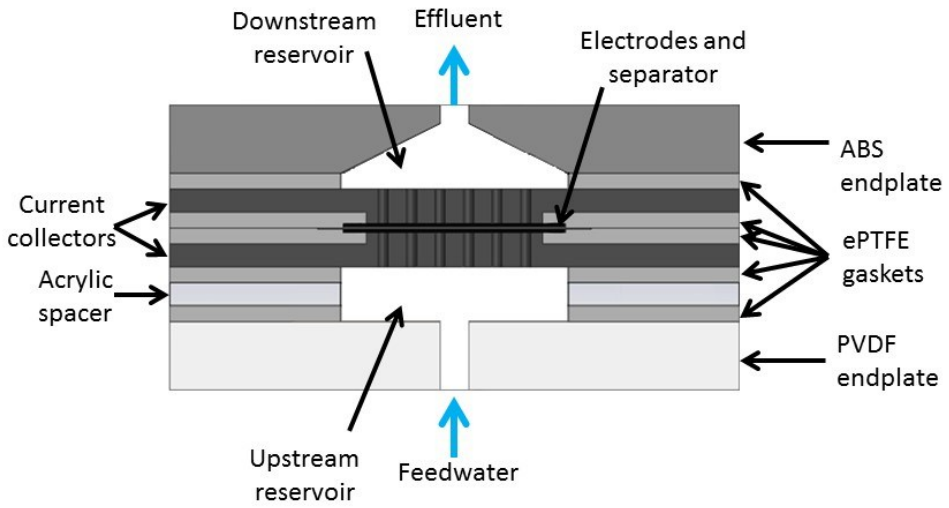

Figure S2 – A schematic of the experimental CDI cell cross section. Dimensions and descriptions of each component are provided in the main text.

The pressure drop across the system is the sum of the pressure drops in each system component, ΔP_i:

$$\Delta P = \sum_i \Delta P_i \,. \qquad \text{* MERGEFORMAT (SI.1)}$$

The pressure drop expressions are listed in Table SI1 for each system component[1,2].

Table S1: Models used for the pressure drop across each cell component in the cell with perforated electrodes.

Component number (*i*)	Component name	Model type	Expression
1	Inlet tube	Poiseuille pipe flow	$\Delta P_1 = \frac{128\mu L_1 Q}{\pi D_1^4}$
2	Upstream reservoir	Sudden expansion into a reservoir	$\Delta P_2 = \frac{\rho Q^2}{2A_{2,1}^2}\left(K_2 - 1 + \beta_2^{-4}\right)$
3	Upstream current collector	Poiseuille bundle of capillaries flow	$\Delta P_3 = \frac{32\mu L_3 Q}{A_f D_3^2 \psi_3}$
4	Electrodes	Poiseuille bundle of capillaries flow	$\Delta P_4 = \frac{32\mu L_4 Q}{A_f D_4^2 \psi_4}$
5	Downstream current collector	Poiseuille bundle of capillaries flow	$\Delta P_5 = \frac{32\mu L_5 Q}{A_f D_5^2 \psi_5}$
6	Downstream reservoir	Contracting conical diffuser	$\Delta P_6 = \frac{\rho Q^2}{2A_{6,2}^2}\left(K_6 + 1 - \beta_6^4\right)$

7	Outlet tubulation	Poiseuille pipe flow	$\Delta P_7 = \frac{128 \mu L_7 Q}{\pi D_7^4}$
8	Outlet tube	Poiseuille pipe flow	$\Delta P_8 = \frac{128 \mu L_8 Q}{\pi D_8^4}$

Symbols

- A_f – cross-sectional flow area (m^2)
- $A_{i,1}$ – component upstream cross-sectional area (m^2)
- $A_{i,2}$ – component downstream cross-sectional area (m^2)
- D_i – tube or perforation diameter (m)
- f – laminar flow friction factor
- K_i – loss coefficient
- L_i – component length along flow direction (m)
- Q – feedwater flow rate (m^3/s)
- α – diffuser angle
- β_i – effective outlet/inlet area ratio
- λ – jet contraction ratio
- μ – feedwater viscosity (Pa s)
- ρ – feedwater density (kg/m^3)
- ψ_i – component porosity

Determination of the two reservoir loss coefficients, K_i, is dependent on the reservoir geometry. The effective area ratio β_i is defined as

$$\beta_i = \sqrt{A_{i,2} / A_{i,1}} \, . \qquad \text{* MERGEFORMAT (SI.2)}$$

The upstream reservoir loss coefficient K_2 may then be calculated as

$$K_2 = \left(1 - \beta_2^{-2}\right)^2 . \qquad \text{* MERGEFORMAT (SI.3)}$$

The downstream reservoir is modeled as a conical reservoir. In this geometry, the jet contraction ratio λ is defined as

$$\lambda = 1 + 0.622 \sin\left(\alpha / 180\right)^{4/5} \left(1 - 0.215\beta^2 - 0.785\beta^5\right). \text{* MERGEFORMAT (SI.4)}$$

The diffuser angle α is 146 degrees. The downstream reservoir loss coefficient K_6 is then calculated as

$$K_6 = 0.0696 \sin\left(\alpha / 2\right)\left(1 - \beta_6^5\right)\lambda^2 + \left(\lambda - 1\right)^2 + \frac{f\left(1 - \beta_6^4\right)}{8 \sin\left(\alpha / 2\right)} \text{* MERGEFORMAT (SI.5)}$$

The friction factor for laminar flow f is calculated at the outlet of the downstream reservoir and is given by

$$f = \frac{64}{\mathrm{Re}} \, . \qquad \text{* MERGEFORMAT (SI.6)}$$

It is important to note that f is a function of the Reynolds number Re and thus varies according to the flow rate Q.

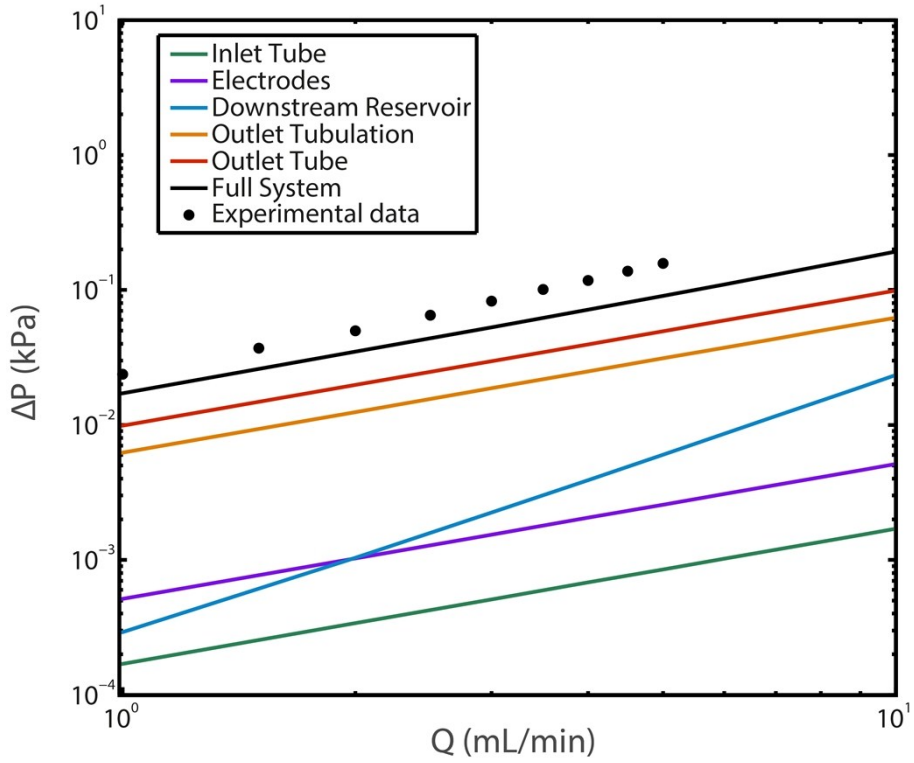

Figure S3 – Plot of the expected pressure drop across each component in the system with perforated electrodes, calculated from the expressions in Table S1. The black line shows the predicted pressure drop across the full system, and the black dots show the experimentally measured feed pressure (both are also shown in Figure 2). The pressure drop across the outlet tubulation and downstream reservoir are predicted to be of the order or higher than that across the perforated electrodes.

SI3: Current response of the CDI cell

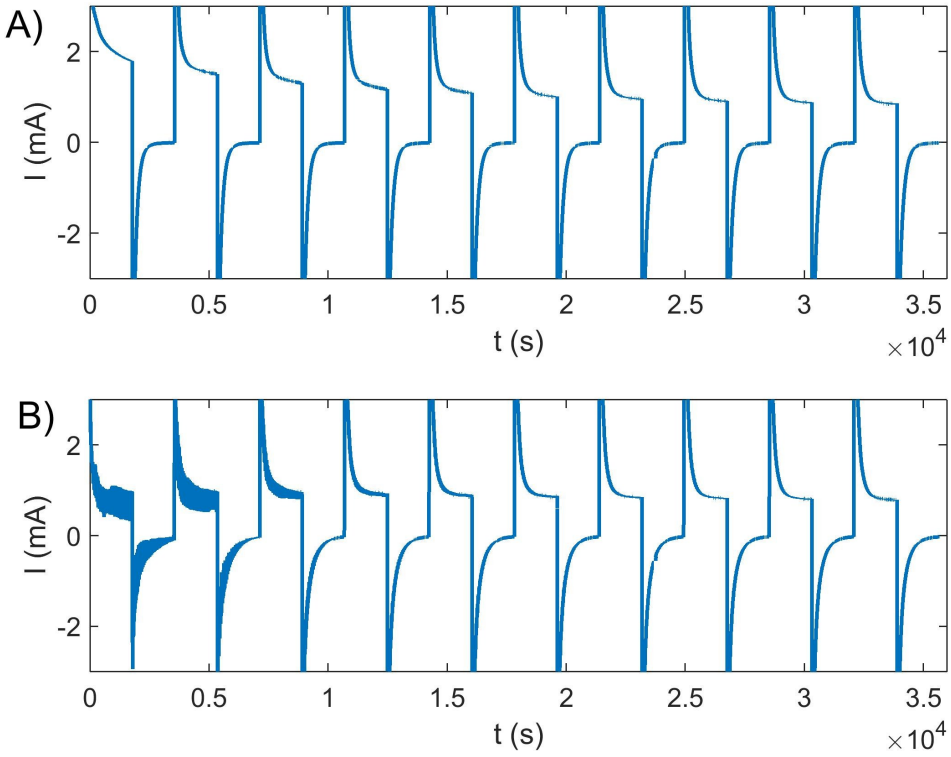

Figure S4 – Measured current response of the CDI cell during cycling at 1.0 V charging/0 V discharging voltages. A) The unperforated electrodes system shows a 1st cycle leakage current of ~1.9 mA, which stabilizes by the 5th cycle to ~1 mA. B) The perforated electrodes system where cycles 4-10 show a leakage current of ~1 mA.

SI4: Overlay of effluent concentration vs. time data

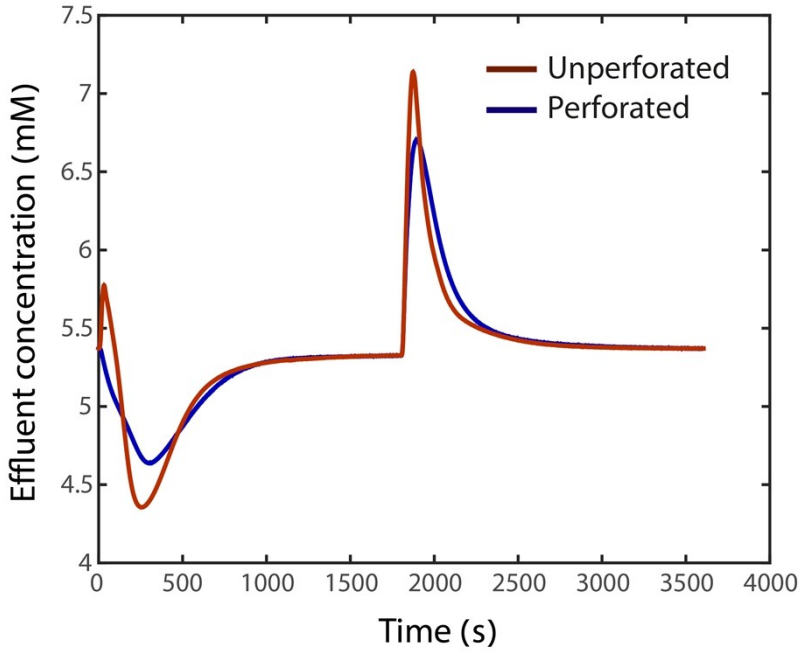

Figure S5 – An overlay of the measured effluent concentration versus time for the 10th cycle shown in Figure 3A and 3B. Features of the cell with unperforated and perforated electrodes can be directly compared, showing sharper features and an inversion peak for the unperforated electrodes.

References

1 D. C. Rennels and H. M. Hudson, *Pipe Flow: A Practical and Comprehensive Guide*, John Wiley & Sons, 2012.

2 S. Yao and J. G. Santiago, *J. Colloid Interface Sci.*, 2003, **268**, 133–142.